ChemCatChem

Research Article
doi.org/10.1002/cctc.202300513

Chemistry Europe
European Chemical Societies Publishing

www.chemcatchem.org

Silver Catalysts Supported on High Surface Area α-Alumina: Effect of Carbohydrate Template Size and Heat Treatment on Phase Purity

Claudia J. Keijzer,[a] Remco Dalebout,[a] Jan Willem de Rijk,[a] John R. Lockemeyer,[b] Tracy L. Lohr,[c] Peter van den Brink,[d] and Petra E. de Jongh*[a]

α-Alumina is a non-porous metal oxide with applications in ceramics and catalysis. Introducing pores into this material to create catalytically relevant surface area is challenging due to phase transitions over a wide temperature range. Current synthesis strategies involve hard templates such as synthetic polymers, e.g. polymethylmethacrylate (PMMA). Here, we compare cellulose and carbonized glucose as low-cost and natural alternative templates for high surface area α-alumina with a two-step heating method. Quantitative XRD was used to methodically investigate alumina phase purity. Increasing the template size in the range of 220–1000 nm improved α-alumina purity from 75 to 98%, while maintaining high surface areas (21–29 $m^2 g^{-1}$). Phase purity increases substantially by prolonging the calcination time. The synthesized high surface area α-alumina was studied as support for silver catalysts in the epoxidation of ethylene and allowed high silver loadings. Ethylene oxide selectivity increased with enhanced α-alumina phase purity. Our 30 wt% silver catalyst on pure high surface area α-alumina did not show loss in selectivity compared to a 15 wt% silver catalyst on commercial non-porous α-alumina. This shows the potential of carbohydrate templates, the importance of templating parameters and the benefits of pure high surface area α-alumina as support for silver catalysts.

Introduction

Alumina is an essential material that is used in refractories, ceramics, and catalysis. Alumina appears in various polymorphs, of which γ-, η-, θ- and α-alumina are most commonly used as catalyst or catalyst carrier.[1] Of these polymorphs, α-alumina is the high temperature crystalline phase and is hard and thermodynamically stable.[2,3] α-Alumina is produced from metastable aluminium (oxide) hydroxides which, upon heating, undergo phase transitions and above 1150–1200 °C form α-alumina.[4,5] At these high temperatures, crystallization occurs which is accompanied by high flux of aluminium and oxygen ions. This high mobility will promote ripening phenomena such as sintering and densification, leading to a significant loss of surface area and porosity.[6] As a result, producing high surface area α-alumina is very challenging. Several methods have been investigated, with for example the use of replicas and hard templates resulting in macroporous α-alumina materials (with specific surface areas ranging from 5–24 $m^2 g^{-1}$ and pore volumes of 0.07–1.2 $cm^3 g^{-1}$).[4,6–10] By carefully choosing a template, it is possible to influence the (macro)pore size and morphology of the resulting metal oxide.[11–14]

In the case of hard templating, latex colloidal crystals have been used as templates for the synthesis of three-dimensionally ordered macroporous (3DOM) metal oxides such as silica and titania.[15–18] Holland *et al.* synthesized macroporous alumina by introducing an aluminium alkoxide precursor to such a template.[19] Although having a high surface area, the alumina was amorphous and exhibited a broad pore size distribution. The same group later succeeded to synthesize a well-defined 3DOM α-alumina by precipitating aluminium hydroxide in the voids of the template followed by calcination.[20] In our group we developed a more advanced synthesis route.[21] According to this route, the sample is heated in inert atmosphere to carbonize the polymer spheres to a carbon coating. This coating stabilizes the γ-alumina that has formed simultaneously, and consequently also protects the pore structure from collapsing. A second heat treatment is performed in oxidizing atmosphere, to remove the carbon coating while γ-alumina is transformed into macroporous α-alumina.[21] This encouraged us to explore other templates that are less costly, time, and energy intensive to produce.

In order to make effective use of this 'carbon-coating' technique, templates require a sufficient amount of carbon.

[a] C. J. Keijzer, Dr. R. Dalebout, J. W. de Rijk, Prof. Dr. P. E. de Jongh
Materials Chemistry and Catalysis
Debye Institute for Nanomaterials Science
Utrecht University
3585 CG Utrecht (The Netherlands)
E-mail: P.E.deJongh@uu.nl
[b] Dr. J. R. Lockemeyer
Shell Global Solutions US Inc.
3333 Highway 6 South, Houston, TX-77082 (USA)
[c] Dr. T. L. Lohr
Shell Catalysts & Technologies
3333 Highway 6 South, Houston, TX-77082 (USA)
[d] Dr. P. van den Brink
Shell Global Solutions International
1031 HW Amsterdam, (The Netherlands)

Supporting information for this article is available on the WWW under https://doi.org/10.1002/cctc.202300513

Carbohydrates are polymerized monosaccharides and are similar in elemental composition to synthetic polymers such as PMMA.[22,23] Cellulose is one of the most abundant natural polymers, consisting of repeating D-glucose monomers.[23] Chemically modified cellulose and nanocellulose aerogel templates have been reported to produce porous γ-alumina and α-alumina rods, respectively.[24,25] In both cases no protective carbon coating step was used, and unfortunately the specific surface area and porosity were only reported for the γ-alumina materials (with BET surface areas of 13–62 $m^2 g^{-1}$) but not for α-alumina. Alternatively, starting with glucose it is possible to build a biobased polymer by polymerization and carbonization,[26] resulting in spheres with diameters in a range of 200–2000 nm.[27–29] Gong *et al.* reported the synthesis of macroporous silica using carbonized glucose spheres,[27] which suggests that application for macroporous α-alumina might also be possible.

An important factor to consider in the synthesis of macroporous α-alumina is phase purity and the characterization thereof. Various polymorphs of alumina exist and can occur during synthesis of α-alumina.[6,30,31] To our knowledge, alumina phase impurities have not been thoroughly quantified in literature covering high surface-area α-alumina synthesis.[6,9,10,20,32,33] Quantitative X-ray diffraction (XRD) *i.e.* Rietveld refinement combined with the use of an internal standard, is a suitable tool for the analysis of samples containing multiple phases, including the presence of amorphous phases.[34,35] The reason why phase quantification in combination with templating is important, is because template morphology may influence the final phase purity due to confinement of transition phases. This was demonstrated for TiO_2 by Zhang *et al.*, where anatase was confined in a hard template which delayed the subsequent formation of rutile.[36] In the case of alumina, the exact mechanism behind the transformation of θ-alumina into α-alumina is not known, but several studies have suggested that in order to form stable α-alumina, θ-alumina crystallites should exceed a certain size (typically above 20 nm).[4,37–41]

Phase purity is of great importance for one of the main applications of α-alumina in catalysis. α-Alumina serves as support for silver particles, used as a catalyst for the epoxidation of ethylene to form ethylene oxide.[42–44] Ethylene oxide can easily isomerize to acetaldehyde, catalyzed by OH groups found on the support,[45] leading to subsequent and undesired total combustion. α-Alumina is preferred as a support because of its low OH group density (1–6 OH nm^{-2}).[46,47] High surface area α-alumina can have clear advantages compared to low surface area α-alumina, such as an increased thermal stability of Ag particles.[48] As other alumina polymorphs exhibit higher OH group densities (10–15 OH nm^{-2} for γ-alumina)[1] and are therefore more reactive, the selectivity towards ethylene oxide is an indirect measure of α-alumina phase purity at the surface.

In this work, we investigate the synthesis of macroporous α-alumina and its phase purity using cellulose and carbonized glucose sacrificial templates. We show the effects of template morphology and calcination time on α-alumina phase purity measured via quantitative XRD. Alumina materials were obtained with specific surface areas of 21–29 $m^2 g^{-1}$, with α-alumina phase purity ranging from 75 to 98%. These materials were used as supports for Ag nanoparticles in the epoxidation of ethylene and compared with a commercially available α-alumina as support.

Results and Discussion

Templates

Various materials were used as templates for the synthesis of macroporous alumina. Figure 1A shows an SEM image of a cellulose template. Cellulose has a fibre-like morphology, which is typical for this plant-based material. The glucose-derived templates (Figure 1B–D) consist of spheres that are interconnected (necked). Increasing the reaction time from 5 to 6 h with a glucose concentration of 0.5 M slightly but significantly increased the sphere size and amount of necking (Figure 1B versus 1 C). According to literature, 0.5 M glucose is the minimum concentration for polymerization and carbonization of glucose.[27,28] Increasing the glucose concentration from 0.5 M (Figure 1C) to 0.7 M (Figure 1D) at 6 hours reaction time enlarged the sphere size and degree of necking.

Table S1 summarizes the reaction conditions and structural properties of selected templates. The cellulose template has a feature size ranging from 100 nm to 1 μm. The carbonized-glucose (CG) templates of 0.5 M glucose heated for 5 h, 0.5 M glucose heated for 6 h and 0.7 M glucose heated for 6 h, contained spheres with an average size of 200, 220 and 310 nm, respectively (Figure 2). Histograms of the sphere diameters are shown in Figure 2, in which they are denoted as CG200, CG220 and CG310. These materials have a similar size range as the PMMA or cellulosic templates reported in literature as being

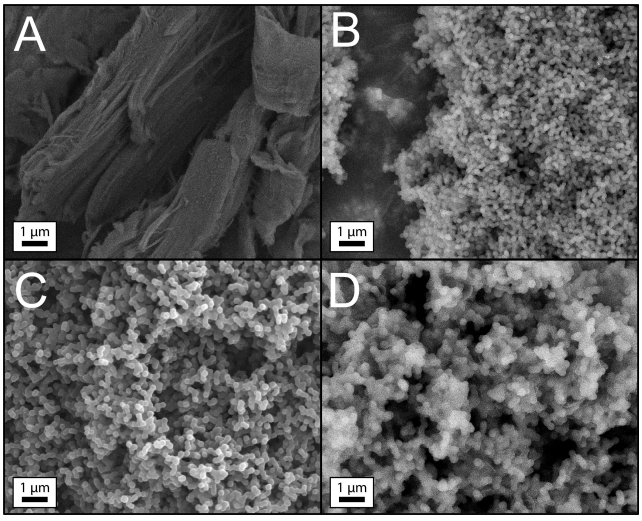

Figure 1. SEM images of cellulose (A) and glucose-derived templates synthesized with the following conditions: 0.5 M glucose heated for 5 h (B), 0.5 M glucose heated for 6 h (C) and 0.7 M glucose heated for 6 h (D).

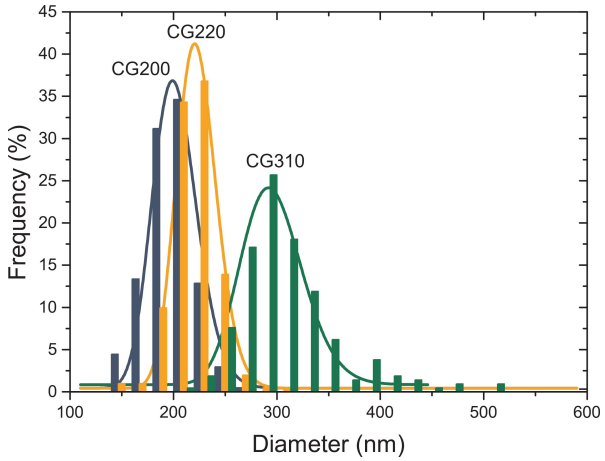

Figure 2. Histograms of measured sphere diameters of templates. The templates are labeled as CG[average sphere size in nm]: CG220, CG220 and CG310. For each sample more than 200 spheres were measured.

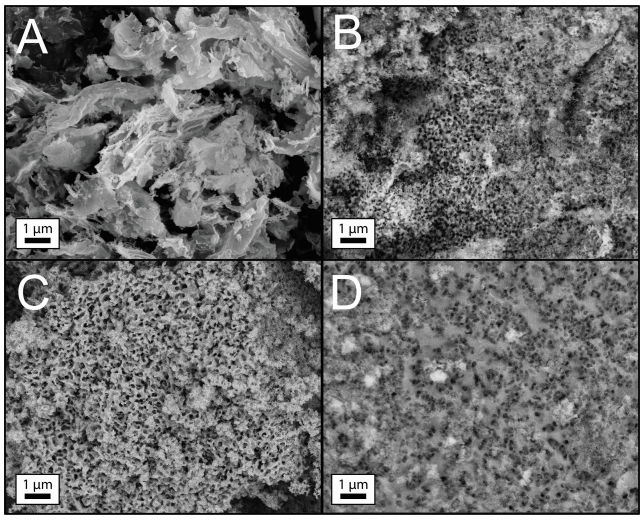

Figure 3. SEM images of alumina templated with microcrystalline cellulose (A), 0.5 M glucose heated for 5 h, CG200 (B), 0.5 M glucose heated for 6 h, CG220 (C) and 0.7 M glucose heated for 6 h, CG310 (D), heated for 6 h in N2 at 1150 °C and calcined for 6 h in air at 1150 °C.

used for the preparation of porous α-alumina.[20,25,48] However, our templates have the advantage of being more practical and less time-intensive to obtain.

Templated Alumina

The templates mentioned above were used for the synthesis of porous alumina. Figure 3 shows SEM images of the resulting alumina materials. When cellulose was used as template (Figure 3A), the alumina showed a mixture of flake-like solid structures, together with more open structures with a fibre-like morphology, with the fibres consisting of small filaments. When carbonized glucose was used as template this resulted in porous materials with connected spherical pores (Figure 3B–D) of uniform size, resembling the inverse of the templates. The morphology of the porous materials obtained from the CG200 and CG220 templates is quite similar. The material obtained from template CG310 exhibits a more open porosity. This is probably due to the fact that CG310 contained some denser domains, leaving larger open spaces once the template was removed.

We used a specific two-step method, that was developed in our group earlier to obtain high quality alumina inverse replicas of the templates.[21] By first heating in inert atmosphere, the carbohydrate template transforms into a carbon coating, protecting the porous structure, which is removed in a subsequent heat treatment in oxidizing atmosphere. TGA showed that during calcination in air, a 70% weight loss was observed between 570 and 650 °C (Figure S4). Moreover, in this temperature range a CO_2 peak was detected with an online MS confirming that this weight loss was caused by removal of the protective carbon coating in a second oxidative step. No weight loss was observed above 650 °C. To our knowledge, this is the first time that carbonized glucose spheres and cellulose were successfully used as templates for the synthesis of porous alumina, using a two-step heating method to obtain high quality replicas of the templates.

N_2- and Ar-physisorption were performed to determine the BET surface area of the alumina materials (Table 1). Isotherms are shown in section B of the Supplementary Information (Figures S1–2) together with additional Hg intrusion and Ar physisorption data of CG310-templated alumina (Figure S3). Based on Hg intrusion, the pore diameter of CG310-templated α-alumina is in the range of 100–1000 nm, which is in the same size range as the spheres of template CG310 (310 nm), indicating that the inverse of the template is achieved throughout the entire sample. The pore volume of this material is 1.85 $cm^3 g^{-1}$, corresponding to a volumetric porosity of 83%, which is extraordinarily high compared to templated alumina materials reported earlier.[6,7,9,10] It is known that the phase transition to α-alumina induces a loss of specific surface area.[6] The alumina materials with equal calcination times (6 h) but produced with different templates (cellulose, CG220 and CG310) have a BET surface area of 21–29 $m^2 g^{-1}$. This is in accordance with literature, where α-alumina was templated with polymer spheres in a similar size range and showed specific surface areas of 20–30 $m^2 g^{-1}$.[20,21,48] It is noteworthy

Table 1. Overview of physisorption data obtained from different alumina supports. The alumina materials are labelled as [template]-[calcination time in air in h]. CG220-12h was characterized with Ar physisorption, all other samples with N2-physisorption.

Material	Template	Calcination time (h)	BET surface area ($m^2 g^{-1}$)
cellulose-6h	cellulose	6	21
CG220-2h	CG220	2	45
CG220-6h		6	29
CG220-12h		12	20
CG310-6h	CG310	6	24

that equally high surface areas can be achieved with these disordered carbohydrate materials. α-Alumina templated with cellulose shows the smallest surface area, which can be explained by the fact that this is a template with large filaments, resulting in larger pores. Cellulose has been used before as template for γ-alumina, resulting in a specific surface area of 33 $m^2 g^{-1}$.[24] Using the two-step heating method, we succeeded to synthesize α-alumina with a similarly high specific surface area as the reported γ-alumina, thereby overcoming the problem of severe loss of specific surface area.

Increasing the calcination time for CG220-templated Al_2O_3 from 2 to 6 h decreased the BET surface area from 45 to 29 $m^2 g^{-1}$, which might have been a result of sintering and/or increased α-alumina content (*vide infra*). For the sample calcined for 12 h, Ar-physisorption pointed to a lower specific surface area of 20 $m^2 g^{-1}$. The SEM measurements (Figure S4) also clearly indicate the presence of a porous structure.

Alumina Phase Quantification

The crystalline phases of CG220-6 h, CG310-6 h, and cellulose-6h were determined with XRD and compared with commercially available α-Al_2O_3 of 1 $m^2 g^{-1}$ (C1) and 8 $m^2 g^{-1}$ (C8) (Figure 4A). In all cases, α-alumina was the dominant phase. The commercial α-alumina materials display the most intense peaks, indicating that these are highly crystalline. In the case of commercial C1, an additional peak around 38° *2θ* is ascribed to the presence of sodium aluminate ($Na_{1.3}Al_{11}O_{17.5}$), probably resulting from impurities introduced during the industrial alumina production.[49]

Only the CG220-templated alumina (CG22020-6 h) diffractogram contains a broad peak around 53° *2θ* (Figure 4A, grey area), indicating the presence of an amorphous phase. Template CG220 was used to investigate the influence of calcination time on phase purity. After the 6 hour heat treatment in N_2, the duration of the heat treatment in air was varied from 2 h to 12 h (Figure 4B). α-Alumina is present in all three materials. However, the intensity of the α-alumina peaks differ greatly: increasing the calcination time enhanced the intensity of the peaks, indicating a higher degree of crystallinity. Moreover, the amorphous peak around 53° *2θ* is present in CG220-2 h and in CG220-6 h, but disappeared after 12 hours of calcination.

Quantitative fitting of XRD patterns was performed to shed light on the exact composition of the templated alumina materials. In section E of the Supplementary Information, diffractograms are shown of the samples containing ZnO as internal standard, as well as the fits (Figures S6 and S7). Table S2 shows an overview of the phase contents. Figure 5 summarizes the results for the commercial α-Al_2O_3 carriers, α-alumina prepared with different templates, and different calcination times.

The commercial samples mostly contained α-alumina. C1 also consisted for 5% of a sodium aluminate phase. The commercial C8 was most pure: no other phases were detected. In the middle section of Figure 5, different templates (CG220, CG310 and cellulose) are compared, all with a calcination time of 6 h. CG220-templated Al_2O_3 (CG220-6 h) and CG310-templated Al_2O_3 (CG310-6 h) mostly consist of α-alumina (75–77%). Both CG310-6 h and CG220-6 h also contain γ-Al_2O_3 (2% versus 11%, respectively), while the first has slightly more θ-Al_2O_3 (7% versus 5%). Both materials also show some amorphous alumina (8–13%). Cellulose-templated Al_2O_3 (cellulose-6h) consists for 98% of α-alumina, and only trace amounts of γ- and θ-alumina. This is probably due to the large feature size of the cellulose template, and hence open structure formed. For instance Gan *et al.* reported that larger (non-porous) alumina precursor particles transformed to α-alumina at slightly lower temperatures than small particles.[50] Interestingly, the 21 $m^2 g^{-1}$ cellulose-6h that we have prepared with our two-step heat treatment method contained a higher percentage of α-alumina (98%) than the commercial 1 $m^2 g^{-1}$ α-alumina samples.

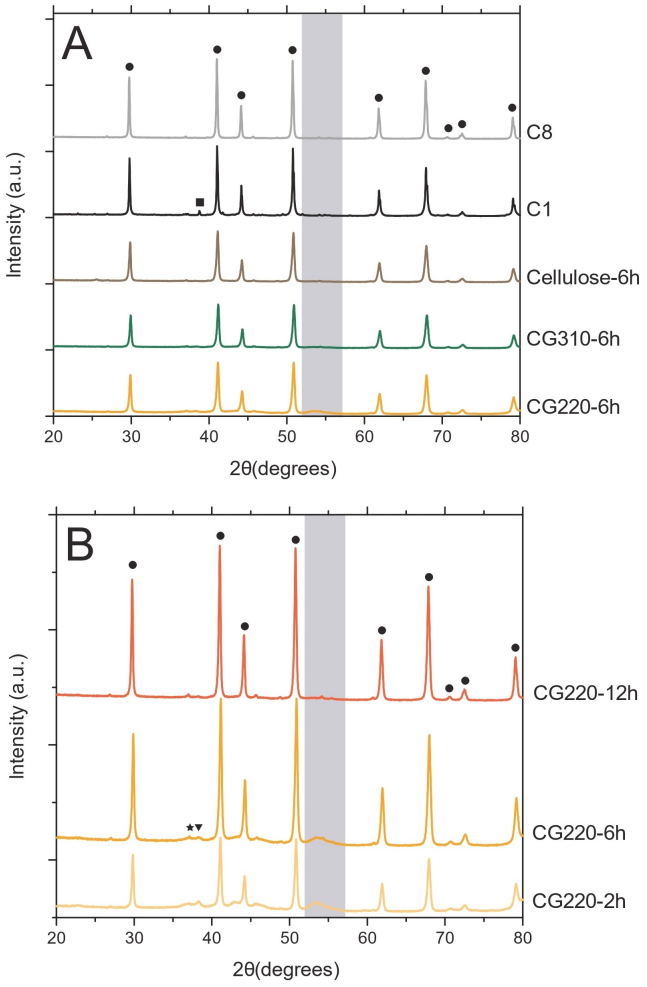

Figure 4. XRD patterns of different α-alumina materials (A) giving an overview for the commercial α-alumina (1 and 8 $m^2 g^{-1}$ are C1 and C8, respectively), cellulose-6h, CG310-6 h and CG220-6h. (B) Zoom in on the carbonized glucose-templated materials, CG220-2 h, CG220-6 h and CG220-12 h. Amorphous bands are highlighted in grey at 53° *2θ*. For clarity, the diffraction angles of α-alumina (●), γ-alumina (★), θ-alumina (▼) and $Na_{1.3}Al_{11}O_{17.5}$ (■) are indicated.

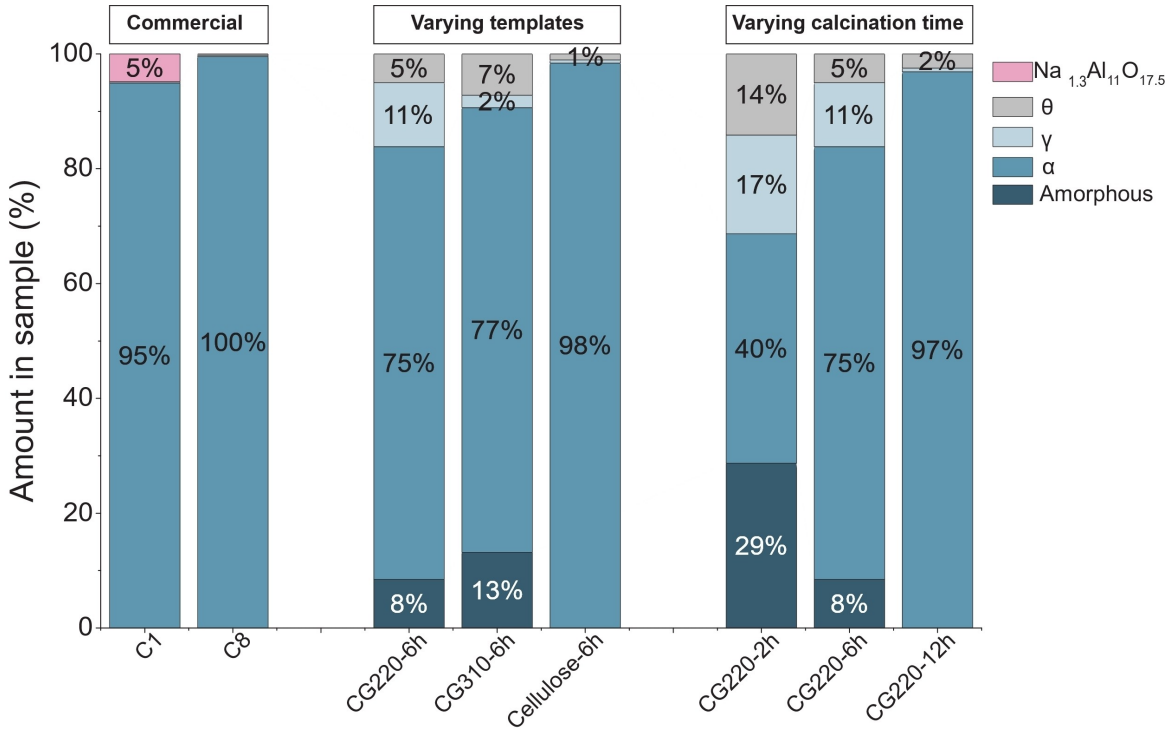

Figure 5. Quantification of alumina phases present in the selected materials. Commercial materials C1 and C8 are shown as a reference. CG310-6h is templated with CG310 and calcined for 6 h, cellulose-6 h is templated with cellulose and calcined for 6 h. CG220-2h, CG220-6h and CG220-12h are templated with CG220 with calcination times of 2, 6 and 12 h, respectively.

The compositions of CG220-templated Al_2O_3 with calcination times of 2, 6 and 12 h are shown in the right section of Figure 5 (CG220-2h, CG220-6h and CG220-12 h, respectively). It is known from literature that heating alumina, without a template, for a longer time can increase the α-alumina content.[51] Indeed, the content of amorphous phase, γ-, and θ-Al_2O_3 decreases accordingly as a result of a longer calcination time. After calcining for 2 h, CG220-2 h consists of 40% α-alumina, 17% γ-alumina, 14% θ-alumina and 29% amorphous phase. Prolonging the calcination time to 6 h and 12 h increases the amount of α-alumina to 75% and eventually to 97% (with trace amounts of γ- and θ-alumina). Hence increasing the calcination time can, even for this relatively fine template that delivers high specific surface area α-alumina, lead to virtually phase pure α-alumina when using our two-step heating method, with the highest heat treatment at 1150 °C. This effect of calcination time on phase purity is interesting, because in earlier studies a variety of templates, calcination times, and temperatures was reported (1–9 h and 1100–1300 °C, respectively) when using a single-step heating method for templated alumina.[6,20,21,24,25,33,48] In these studies, calcination times were not investigated and it was simply assumed that there was a complete transition to α-alumina. However, here we demonstrate that after 6 h a significant amount of phase impurities is still present in the alumina materials that are templated with 220–310 nm features. This is the first time that the influence of template and calcination conditions on alumina phase purity are systematically investigated through quantification with XRD.

Silver Nanoparticle Deposition for Ethylene Epoxidation

Silver nanoparticles were deposited with loadings of 15 wt% and 30 wt% Ag on selected supports: C8, cellulose-6h and CG220-6h. The commercial 1 $m^2 g^{-1}$ α-alumina was not used because of the presence of the sodium aluminate phase, as sodium is known to influence the catalysis.[52,53] The silver particle sizes were determined with SEM. In Figure 6, SEM images of 15 and 30 wt% Ag supported on C8, cellulose-6h and on CG220-6h are depicted: silver particles are bright white and spherical. As can be seen in the SEM image, the templated alumina supports had retained their morphology during the impregnation, drying and calcination steps. A zoomed-out SEM image of 15Ag50/CG220-6h can be found in the Supporting Information (Figure S10). The silver particles had surface averaged sizes of 47 to 73 nm (Table 2). We specifically chose this size range as unpromoted silver particles in the range of 50–70 nm are known to exhibit optimal activity which is believed to be the result of the presence of (sub)surface oxygen in particles with such extended facets.[47,54–56] 15Ag50/C8 was prepared in an inert atmosphere to limit the degree of sintering on this lower surface area support and hence attain similar particle sizes as for the other catalysts. Additionally, catalysts were characterized with SEM after the reaction (Figure S11) and showed Ag particles in the range of 70–80 nm (Figure S12), which means that dynamic evolution of silver species resulted in similar particle sizes. The fraction of Ag atoms is not less for the 30 wt% Ag catalysts.

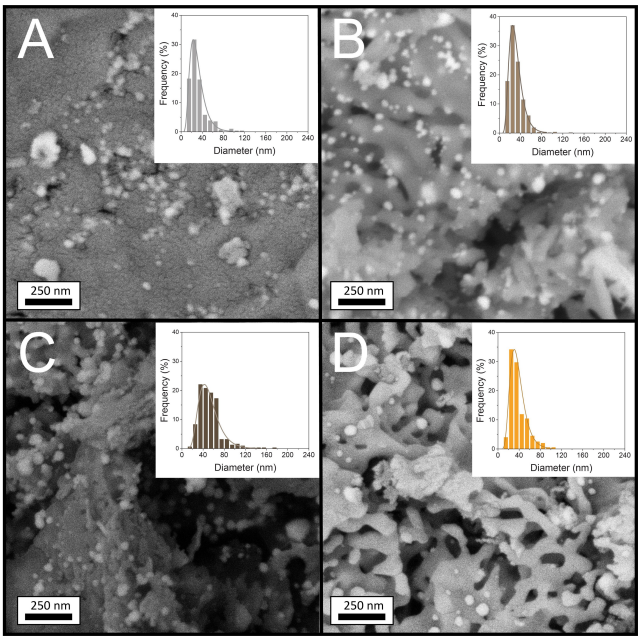

Figure 6. SEM images of 15 wt% Ag on C8 (A), on cellulose-6 h (B), 30 wt% Ag supported on cellulose-6 h (C) and on CG220-6h (C). Corresponding histograms with particle size distributions are shown as insets.

The alumina-supported silver catalysts (Table 2) were tested in the ethylene epoxidation reaction, which is one of the largest processes within the petrochemical industry, and a very sensitive test reaction to test the various inert supports. It typically runs with α-Al_2O_3-supported Ag catalysts, and the selectivity is known to depend critically on the surface properties of the α-Al_2O_3 support and hence its phase purity.[46] Catalytic tests were performed at 215 °C and, as typically done in industry, in the presence of chloride. Since the catalysts have different silver loadings (15 and 30 wt%), the catalyst loading was adjusted to 15 mg Ag per catalytic run, which means that less total catalyst weight was loaded if it contained more wt% silver. High Ag loadings are not a problem for practical reactor design, as current industrial catalysts consist of similarly high Ag loadings on low surface area supports.[53] The gas flow rate per g Ag was kept constant at 132 $L\,g_{Ag}^{-1}\,h^{-1}$.

During the first 10–15 h, the catalysts went through an stabilization period (Figure S8), which is expected if chloride is present.[57] Conversion and ethylene oxide selectivity data of the catalysts after this activation period are summarized in Table 3. The results show that ethylene conversion was similar for the different catalysts (2.8–3.6%), which is important as the selectivity is known to depend on (decrease with) increasing conversion.[47] Based on the conversion after 16 hours, apparent turnover frequencies (TOFs) of 0.015–0.021 $mol_{ethylene}\,mol_{Ag,surface}^{-1}\,s^{-1}$ were determined for the catalysts, which is in line with literature (0.014–0.15 s^{-1}).[58]

Differences in selectivity may be expected for the different alumina supports, as it is known that a sequential reaction takes place over the support surface groups (*e.g.* Al–OH groups) that cause a loss of selectivity.[46] When comparing catalysts with similar weight loading (15 wt% silver) but two different specific surface areas (8 $m^2\,g^{-1}$ and 21 $m^2\,g^{-1}$ for 15Ag50/C8 vs. 15Ag50/cellulose-6h, Table 3), we see that selectivity was 78% for the lower surface area and 67% for the higher surface area support. Based on XRD there is no significant difference in phase purity in C8 and cellulose-6h (100% vs. 98%), therefore, the selectivity difference is most likely caused by the difference in specific surface area of the α-alumina support. This is in line with earlier studies that reported lower selectivities for higher surface area α-alumina supported silver catalysts.[45,46,48,59] However, these studies did not report phase compositions of the used α-alumina supports. Comparing silver loadings of 30 wt% on two different high-surface area α-alumina support with different phase purity (30Ag50/CG220-6h vs. 30Ag70/cellulose-6h) resulted in very different selectivities: 30Ag50/CG220-6h showed a 56% selectivity to ethylene oxide, when 30Ag70/cellulose-6h was 78% selective. The surface areas (29 $m^2\,g^{-1}$ vs. 21 $m^2\,g^{-1}$) are similar. This indicates that the 25% phase impurities in CG220-6h (γ-, θ- and amorphous alumina with higher OH concentrations) could explain the lower ethylene oxide selectivity. This is also complemented by the 40% acetaldehyde for 30Ag50/CG220-6h compared to 10% acetaldehyde selectivity for 30Ag70/cellulose-6h (Figure S8), with which we emphasize the importance of using pure α-alumina. Moreover, we express the relevance of reporting the alumina phase purity besides specific surface area for a fair comparison between α-alumina supported silver catalysts.

Having high surface area α-alumina is expected to allow a higher Ag loading without compromising the Ag particle size. Doubling the weight loading on the same high surface-area support (15Ag50/cellulose-6h and 30Ag70/cellulose-6h) resulted only in a 50% increase in Ag particle size (47 to 73 nm) but an increased selectivity from 67% to 78%. The explanation for this is that with a higher silver loading less OH groups are

Table 2. Overview of alumina supported silver catalysts used for catalytic testing. Materials are labelled as [*wt% silver*] Ag[$d_{p,s}$]/[*template*]-[*calcination time in hour*]. C8 is the commercial α-Al_2O_3 support. Decomposition of the silver precursor of 15 Ag50/C8 was in an atmosphere of N_2, whereas the other impregnated supports were treated in 25% O_2 in N_2.

Material	Ag loading (wt %)	Ag particle particle size $d_{p,s}$ (nm)	α-Al_2O_3 BET surface area ($m^2\,g^{-1}$)
15Ag50/C8	15.0	52 ± 26	8
15Ag50/cellulose-6h	16.1	47 ± 20	21
30Ag70/cellulose-6h	31.5	73 ± 30	21
30Ag50/CG220-6h	29.4	53 ± 22	29

Table 3. Conversion and selectivity data of the 15 wt% and 30 wt% silver on α-alumina catalysts, labelled as [*wt% silver*]Ag[$d_{p,s}$]/[*template*]-[*calcination time in hour*]. Datapoints between 16 and 20 hours were averaged.

Catalyst	Ethylene conversion (%)	Ethylene oxide selectivity (%)
15Ag50/C8	3.5 ± 0.07	78 ± 1.7
15Ag50/cellulose-6h	3.6 ± 0.22	67 ± 2.6
30Ag70/cellulose-6h	2.8 ± 0.05	78 ± 3.7
30Ag50/CG220-6h	2.8 ± 0.03	56 ± 4.6

exposed on the support surface. In other words, the ratio between the undesired side reaction on alumina surface groups and the desired formation of ethylene oxide on the silver particles, which is an important parameter for the overall selectivity to ethylene oxide, is shifted towards the formation of ethylene oxide. This also clearly illustrates the great benefit of preparing high surface area and almost phase-pure α-alumina supports. The higher specific surface area allows to load a higher silver weight loading, and means that overall with the same amount of Ag similar conversions can be reached with the same selectivity, while using less support and total catalyst weight. For instance, we observe a similar high selectivity comparing catalysts supported on low surface area α-alumina (15 Ag65/C8) with pure high surface-area α-alumina and double the silver loading (30Ag70/cellulose-6h). It is a remarkable result that an almost three times increase in specific surface area with our templating route does not lead to a lower selectivity.

Conclusions

High quality and high surface area α-alumina materials were synthesized with templates containing carbonized glucose spheres and cellulose using a two-step heating method. The use of carbonized spheres-based templates resulted in 75–77% α-alumina purity, while a cellulose-based template, displaying larger features than the carbonized spheres, resulted in 98% α-alumina. We also showed that phase purity can be increased by prolonging the calcination time of the two-step heating method. This is an important aspect of templated alumina which enables smaller templates to be explored in the future. Phase purity quantification led to a direct comparison between α-alumina supported silver catalysts, and an increased phase purity clearly enhanced the selectivity towards ethylene oxide. High surface area α-alumina allowed for an increase in silver loading and because of its high phase purity, our cellulose-templated α-alumina resulted in a similar ethylene oxide selectivity as a reference catalyst supported with low surface area α-alumina. This study illustrates both the potential of carbohydrates as (precursors of) templates, and the importance of template and heating conditions for the synthesis of pure α-alumina with a high surface area.

Experimental Section

Synthesis of Templated Alumina

Several materials were used as sacrificial templates for the synthesis of α-alumina. Microcrystalline cellulose powder (≥99%, Sigma-Aldrich) was used as received. A second type of template was synthesized by polymerization and carbonization of glucose.[28] 10.1 g or 12.6 g D(+)-glucose (96%, Sigma-Aldrich) was dissolved in 100 mL milliQ water. The glucose solution was transferred to a 250 mL Teflon-lined autoclave, which upon closing was heated in air at 180 °C for 5–6 hours. The resulting dispersion was filtered in a Büchner funnel, and a brown solid material was obtained and used as template.

The synthesis of macroporous alumina was based on a previously developed procedure.[21] In a typical synthesis, 2 g of template was placed in a Büchner funnel. The template was first wetted for 2 minutes with 6 mL 1 M aluminium nitrate nonahydrate (≥99%, Fisher) solution in milliQ water/methanol (99.9%, VWR) (1:1 vol ratio) and then with 6 mL of an ammonia (28–30 wt%, Emsure)/methanol (1:1 vol ratio) solution. After each wetting step, the sample was dried in vacuum for 10 minutes. Once the template was wetted three times with each solution, the material was dried overnight in air at room temperature. The dried material was heated to 1150 °C for 6 hours in a nitrogen flow (5 °C min^{-1}, flow rate of 4 L $g_{material}^{-1}$ h^{-1}), cooled down to room temperature, and heated to 1150 °C for 2 h, 6 h or 12 h in air with a similar ramp and flow rate as the previous step. This specific sequence of first heating in inert atmosphere, and then in oxidizing atmosphere allows the formation of a carbon protective shell from the carbohydrate template that stabilizes the structure during heating, and which is later removed in the second oxidative heat treatment.[21]

Silver Deposition

Silver nanoparticles were deposited onto the α-alumina carriers through incipient wetness impregnation, based on a procedure described elsewhere.[47] In addition to the templated alumina materials, an 8 m^2 g^{-1} α-alumina (Al-4196, supplied by BASF) material was used as support. Silver oxalate was used as silver precursor, which was synthesized prior to the impregnation. Typically, an aqueous solution of silver nitrate (≥99.0%, Sigma-Aldrich) was added to a 60 °C aqueous solution of oxalic acid (≥99.0%, Sigma-Aldrich) (2:1 mol ratio). The white silver oxalate precipitate was centrifuged and washed three times in milliQ water and once in ethanol, after which it was left to dry overnight at 60 °C in air.

Prior to the incipient wetness impregnation, the alumina powders were dried in vacuum at 200 °C for 2 h. Silver oxalate was dissolved in a mixture of milliQ water/ethylenediamine (99%, Sigma-Aldrich) (4:1 mol ratio), and the dried powder was impregnated with this solution up till 90% of its pore volume, aiming for a silver loading of 15 or 30 wt%. The impregnated material was left to dry overnight at 60 °C in static air, and was mixed thoroughly after 10, 30 and 45 min of drying. The silver precursor was decomposed at 215 °C (5 °C min^{-1}) for 2 h in N_2 or in 25% O_2 in N_2 (7000 hr^{-1}).

Characterization

The templates, support materials and supported silver catalyst materials were analyzed with scanning electron microscopy (SEM) using a FEI Helios G3 UC microscope, operated at 5–10 kV. A sticky carbon tape was used to attach the sample powder to the sample holder. The sample was covered with a 7.5 nm PdPt layer through sputter coating prior to the SEM measurement. A minimum of 200 silver particles were analyzed per sample using ImageJ software. From these measurements, the surface-averaged particle size ($d_{p,s}$) and standard deviations ($\sigma_{p,s}$) were calculated (Equation 1).

$$d_{p,s} \pm \sigma_{p,s} = \frac{\sum_{i=1}^{n} d_i^3}{\sum_{i=1}^{n} d_i^2} \pm \sqrt{\frac{1}{n} \cdot \sum_{i=1}^{n} \left(d_{p,s} - d_i\right)^2} \quad (1)$$

The crystalline phase of the alumina materials was determined with X-ray diffraction (XRD) on a Bruker D2 Phaser diffractometer

equipped with a Co K_α source ($\lambda = 0.1789$ nm), in a range of 20–80° in 2θ (increment 0.020°, 1 s step^{-1}, 30 kV, 10 mA). In order to determine the phase contents in the templated alumina materials, an internal standard (zinc oxide) was used. Zinc oxide (99.999%, ABCR GmbH) and the alumina materials were sieved to a 38–75 μm fraction, after which the ZnO was added to the alumina (1:2 mass ratio) and mixed in an agate mortar for 20 min. The obtained diffractograms were compared with crystal structures from the PDF-4+ 2016 database and analyzed with Bruker TOPAS software. Refinements were performed with a first order Chebychev background and a Lorentzian peak fit was used. Details can be found in section E of the Supporting Information.

The BET surface area of the α-alumina materials was determined with N_2-physisorption on a Micromeritics TriStar 3000 instrument, by fitting the experimental data between 0.05 and 0.25 p/p_0. Prior to the measurement, the materials were dried overnight in vacuum at 300 °C. Ar physisorption was performed on a Micromeritics 3Flex instrument. Prior to the measurement, a drying step of 16 h was performed at 350 °C in vacuum. Mercury intrusion porosimetry was performed using a Micromeritics AutoPore V 9600. Prior to the measurement, a drying step of 1 h was performed in nitrogen flow at 400 °C. The pore volume was calculated in the range of 0.1–420 MPa, assuming a contact angle of 140° between the sample material and the mercury.

Thermogravimetric analysis (TGA) was performed on a PerkinElmer TGA 8000 apparatus with an online mass spectrometer (MS) to monitor the removal of the sacrificial template during heat treatment. 8–10 mg of sample was heated from 30 °C to 1200 °C (10 °C min^{-1}) in 100 mL min^{-1} Ar or 20 vol% O_2 in Ar to resemble the two heat treatments in inert atmosphere and in air.

Surface (OH) group densities on the alumina materials were determined with NH_3 temperature programmed desorption (TPD) on a Micromeritics Autochem II 2920 V4.03 instrument. 75–100 mg of support material was heated in 50 mL min^{-1} air at 400 °C for 15 min, prior to a treatment of 10% NH_3 in He at 100 °C for 20 min (25 mL min^{-1} STP). The actual TPD measurement was performed by heating the sample from 100 to 600 °C with a heating ramp of 10 °C min^{-1} in He (25 mL min^{-1}), and the amount of desorbed NH_3 was detected with a thermal conductivity detector (TCD). The amount of surface OH groups was calculated by deconvoluting the complex TPD profile, using Gaussian peak fits. The total peak area was used to calculate the surface OH group density.

Catalytic Measurements

The supported silver particles were tested as catalysts for the epoxidation of ethylene. Typically, 50 or 100 mg catalyst (90–150 μm sieve fraction) was diluted with 250 or 500 mg SiC (212–425 μm). Since the catalysts have different silver loadings (15 and 30 wt%), the catalyst loading was adjusted to test 15 mg Ag per run, with a constant gas flow rate per g Ag of 132 L g_{Ag}^{-1} h^{-1}. The diluted catalysts were loaded in a plug-flow quartz reactor (4 mm diameter) between two layers of quartz wool. The SiC had been washed in HNO_3 (65%, AnalaR Normapur®, 10 mL g_{SiC}^{-1}) and calcined at 800 °C to remove organic and inorganic impurities. The catalysts were tested at 215 °C, after a heating ramp of 10 °C min^{-1}, in a flow of 7.5 vol% ethylene, 2.1 vol% oxygen, 1.8 ppm ethyl chloride in He for 20 hours. As pure silver catalysts have little selectivity response to changing chloride levels,[60] the ethyl chloride concentration was kept constant across all catalysts. The catalysts were evaluated at ethylene conversions as similar as possible (within ca. 3%) when comparing selectivities. Every 15 min, reaction products were analyzed with an online Interscience Compact GC supplied with two separate channels (Porabond Q column and Molsieve 5 A column). Selectivity, ethylene conversion and carbon balance were calculated using Equations 2–4. Calculations on transfer limitations can be found in the Supporting Information, Section F, and clearly indicate that no mass or heat transfer limitations are expected in our systems.

$$Conversion_{Ethylene} = \frac{0.5 \cdot p_{CO_2} + p_{Ethylene\ oxide} + p_{Acetaldehyde}}{p_{Ethylene_0}} \cdot 100\,\% \quad (2)$$

$$Selectivity_{Ethylene\ oxide} = \frac{p_{Ethylene\ oxide}}{p_{Ethylene\ oxide} + 0.5 \cdot p_{CO_2} + p_{Acetaldehyde}} \cdot 100\,\% \quad (3)$$

$$Carbon\ balance = \frac{p_{Ethylene_{out}} + 0.5 \cdot p_{CO_2} + p_{Ethylene\ oxide} + p_{Acetaldehyde}}{p_{Ethylene_0}} \cdot 100\,\% \quad (4)$$

p_x is the partial pressure of molecule x (in Pa). The carbon balance was 100 ± 3% for all datapoints. Apparent turnover frequency (*TOF*) was calculated with Equation 5.

$$TOF = \frac{P \cdot u_{Ethylene} \cdot Conversion_{Ethylene}}{RT} \cdot \frac{A_{Ag,\,atom} \cdot d_{p,s}}{M_{Ag} \cdot 6V_{Ag,\,atom}} \quad (5)$$

P is pressure (1.01×10^5 Pa), u the flow rate of ethylene (m^3 s^{-1}), R is the gas constant (8.31 J mol^{-1} K^{-1}), T is the temperature (298 K), $A_{Ag,atom}$ is the surface area of a silver atom (in m^2), $d_{p,s}$ is the surface averaged silver particle size, M_{Ag} is the mass of silver present in the loaded catalyst (in mol) and $V_{Ag,\,atom}$ is the volume of a silver atom (in m^3). It is important to keep in mind that this TOF calculation is based on the assumption of spherical silver particles and that the surface atoms of the silver particles are the only active sites in the reaction.[48]

Acknowledgements

This work was a collaboration with Shell Global Solutions. CJK was funded via the Advanced Research Center for Chemical Building Blocks consortium, which is co-founded and co-financed by the Dutch Research Council (NWO) and the Netherlands Ministry of Economic Affairs and Climate Policy. Electron microscopy measurements were performed within the Electron Microscopy Centre at Utrecht University. The authors would like to thank Suzan Schoemaker (N_2-physisorption), Dennie Wezendonk (TGA-MS), Eric Hellebrand (SEM), Yuang Piao and Luc Smulders (NH_3-TPD) together with Alice van Velthuijsen, Simon Papa, Desmond Dekker and Arend-Jan van Welsenes (Ar physisorption and Hg intrusion) for technical support.

Conflict of Interests

The authors declare no conflict of interest.

Data Availability Statement

The data that support the findings of this study are available from the corresponding author upon reasonable request.

Keywords: α-alumina · high surface area · phase purity · ethylene epoxidation

[1] I. Chorkendorff, J. W. Niemantsverdriet, *Concepts of Modern Catalysis and Kinetics*, Wiley-VCH, **2007**, p. 189.
[2] G. Busca, *Advances in Catalysis: Structural, Surface, and Catalytic Properties of Aluminas*, Elsevier Inc. **2014**, *57*, p. 330.
[3] C. Piconi, *in Compr. Biomater.*, Elsevier Ltd., **2011**, pp. 73–94.
[4] S. Carstens, R. Meyer, D. Enke, *Materials (Basel)* **2020**, *13*.
[5] Y. Cesteros, P. Salagre, F. Medina, J. E. Sueiras, *Chem. Mater.* **1999**, *11*, 123–129.
[6] T. Kimura, H. Maruoka, *Chem. Commun.* **2019**, *55*, 10003–10006.
[7] S. Carstens, D. Enke, *J. Eur. Ceram. Soc.* **2019**, *39*, 2493–2502.
[8] S. Deville, E. Saiz, A. P. Tomsia, *Acta Mater.* **2007**, *55*, 1965–1974.
[9] M. M. Martín-Ruiz, L. A. Pérez-Maqueda, T. Cordero, V. Balek, J. Subrt, N. Murafa, J. Pascual-Cosp, *Ceram. Int.* **2009**, *35*, 2111–2117.
[10] L. L. Pérez, V. Zarubina, H. J. Heeres, I. Melián-Cabrera, *Chem. Mater.* **2013**, *25*, 3971–3978.
[11] A. R. Studart, U. T. Gonzenbach, E. Tervoort, L. J. Gauckler, *J. Am. Ceram. Soc.* **2006**, *89*, 1771–1789.
[12] D. Gu, F. Schüth, *Chem. Soc. Rev.* **2014**, *43*, 313–344.
[13] Z. Sun, Y. Deng, J. Wei, D. Gu, B. Tu, D. Zhao, *Chem. Mater.* **2011**, *23*, 2176–2184.
[14] S. W. Bian, Y. L. Zhang, H. L. Li, Y. Yu, Y. L. Song, W. G. Song, *Microporous Mesoporous Mater.* **2010**, *131*, 289–293.
[15] O. D. Velev, T. A. Jede, R. F. Lobo, A. M. Lenhoff, *Nature* **1997**, *389*, 447–448.
[16] O. D. Velev, T. A. Jede, R. F. Lobo, A. M. Lenhoff, *Chem. Mater.* **1998**, *10*, 3597–3602.
[17] R. C. Schroden, M. Al-Daous, C. F. Blanford, A. Stein, *Chem. Mater.* **2002**, *14*, 3305–3315.
[18] R. C. Schroden, N. Balakrishnan, *Opal and Inverse Opal Photonic Crystals* **2001**.
[19] B. T. Holland, C. F. Blanford, T. Do, A. Stein, *Chem. Mater.* **1999**, *11*, 795–805.
[20] S. Sokolov, D. Bell, A. Stein, *J. Am. Ceram. Soc.* **2003**, *86*, 1481–1486.
[21] J. E. van den Reijen, P. H. Keijzer, P. E. de Jongh, *Materialia* **2018**, *4*, 423–430.
[22] J. E. Mark, *Polymer Data Handbook* Oxford University Press, **1999**, pp. 39–48, 655–657.
[23] D. Klemm, B. Heublein, H. P. Fink, A. Bohn, *Angew. Chem. Int. Ed.* **2005**, *44*, 3358–3393.
[24] I. S. Martakov, P. V. Krivoshapkin, M. A. Torlopov, E. F. Krivoshapkina, *Fibers Polym.* **2015**, *16*, 975–981.
[25] S. H. Kenawy, M. L. Hassan, *Heliyon* **2019**, *5*, e01816.
[26] G. Ischia, M. Cutillo, G. Guella, N. Bazzanella, M. Cazzanelli, M. Orlandi, A. Miotello, L. Fiori, *Chem. Eng. J.* **2022**, *449*, 137827.
[27] Y. Gong, L. Xie, H. Li, Y. Wang, *Chem. Commun.* **2014**, *50*, 12633–12636.
[28] X. Sun, Y. Li, *Angew. Chem. Int. Ed.* **2004**, *43*, 597–601.
[29] M. Sevilla, A. B. Fuertes, *Chem. A Eur. J.* **2009**, *15*, 4195–4203.
[30] I. Levin, D. Brandon, *J. Am. Ceram. Soc.* **2005**, *81*, 1995–2012.
[31] S. Lamouri, M. Hamidouche, N. Bouaouadja, H. Belhouchet, V. Garnier, G. Fantozzi, J. F. Trelkat, *Bol. La Soc. Esp. Ceram. Y Vidr.* **2017**, *56*, 47–54.
[32] T. Delbrücke, R. A. Gouvêa, M. L. Moreira, C. W. Raubach, J. A. Varela, E. Longo, M. R. F. Gonçalves, S. Cava, *J. Eur. Ceram. Soc.* **2013**, *33*, 1087–1092.
[33] M. Nguefack, A. F. Popa, S. Rossignol, C. Kappenstein, *Phys. Chem. Chem. Phys.* **2003**, *5*, 4279–4289.
[34] A. G. De La Torre, S. Bruque, M. A. G. Aranda, *J. Appl. Crystallogr.* **2001**, *34*, 196–202.
[35] S. T. Misture, *in Encycl. Mater. Tech. Ceram. Glas.*, Elsevier, **2021**, pp. 549–559.
[36] Z. Zhang, F. Zuo, P. Feng, *J. Mater. Chem.* **2010**, *20*, 2206–2212.
[37] P. L. Chang, F. S. Yen, K. C. Cheng, H. L. Wen, *Nano Lett.* **2001**, *1*, 253–261.
[38] Y. Huang, X. Peng, X. Q. Chen, *J. Alloys Compd.* **2021**, *863*, 158666.
[39] H. L. Wen, F. S. Yen, *J. Cryst. Growth* **2000**, *208*, 696–708.
[40] R. B. Bagwell, G. L. Messing, P. R. Howell, *J. Mater. Sci.* **2001**, *36*, 1833–1841.
[41] F. Schüth, *Angew. Chem. Int. Ed.* **2003**, *42*, 3604–3622.
[42] J. R. Lockemeyer, *Process for Preparing a Catalyst, the Catalyst, and a Use of the Catalyst* **2005**, US 2005/0222442A1.
[43] J. G. Serafin, A. C. Liu, S. R. Seyedmonir, H. Soo, T. Szymanski, *Catalysts Having Enhanced Stability, Efficiency and/or Activity for Alkylene Oxide Production* **2006**, *EP1* 675678B1.
[44] T. Pu, H. Tian, M. E. Ford, S. Rangarajan, I. E. Wachs, *ACS Catal.* **2019**, 10727–10750.
[45] J. K. Lee, X. E. Verykios, R. Pitchai, *Appl. Catal.* **1988**, *44*, 223–237.
[46] J. E. van den Reijen, W. C. Versluis, S. Kanungo, M. F. D'Angelo, K. P. de Jong, P. E. de Jongh, *Catal. Today* **2019**, *338*, 31–39.
[47] J. E. van den Reijen, S. Kanungo, T. A. J. Welling, M. Versluijs-Helder, T. A. Nijhuis, K. P. de Jong, P. E. de Jongh, *J. Catal.* **2017**, *356*, 65–74.
[48] P. H. Keijzer, J. E. van den Reijen, C. J. Keijzer, K. P. de Jong, P. E. de Jongh, *J. Catal.* **2022**, 534–544.
[49] M. Authier-Martin, G. Forte, S. Ostap, J. See, *Mineralogy* **2001**, *53*, 36–40.
[50] B. K. Gan, I. C. Madsen, J. G. Hockridge, *J. Appl. Crystallogr.* **2009**, *42*, 697–705.
[51] M. Takht Ravanchi, M. Rahimi Fard, S. Fadaee Rayeeni, F. Yaripour, *Chem. Eng. Commun.* **2015**, *202*, 493–499.
[52] M. Huš, A. Hellman, *J. Catal.* **2018**, *363*, 18–25.
[53] M. Matusz, R. L. Paddock, R. C. Yeates, J. R. Lockemeyer, *Methods for Conditioning an Ethylene Epoxidation Catalyst and Associated Methods for the Production of Ethylene Oxide* **2021**, *EP3* 548471B1.
[54] J. K. Lee, X. E. Verykios, R. Pitchai, *Appl. Catal.* **1989**, *50*, 171–188.
[55] A. J. F. Van Hoof, *Structural Changes in Ethylene Epoxidation Catalysts Investigated by Transmission Electron Microscopy Structural Changes in Ethylene Epoxidation Catalysts Investigated by Transmission Electron Microscopy*, Technische Universiteit Eindhoven, **2019**, pp. 73–80.
[56] M. O. Özbek, I. Önal, R. A. van Santen, *ChemCatChem* **2013**, *5*, 443–451.
[57] J. T. Jankowiak, M. A. Barteau, *J. Catal.* **2005**, *236*, 379–386.
[58] S. T. Oyama, *Mechanisms in Homogeneous and Heterogeneous Epoxidation Catalysis, 1st edition*, Elsevier B. V. **2008**, p. 13.
[59] C. F. Mao, M. Albert Vannice, *Appl. Catal. A* **1995**, *122*, 61–76.
[60] J. R. Lockemeyer, T. L. Lohr, *ChemCatChem* **2023**, 1–6.

Manuscript received: April 6, 2023
Revised manuscript received: June 15, 2023
Accepted manuscript online: June 15, 2023
Version of record online: July 18, 2023